Journal of Power Sources 530 (2022) 231275

Contents lists available at ScienceDirect

Journal of Power Sources

journal homepage: www.elsevier.com/locate/jpowsour

Issues regarding bipolar plate-gas diffusion layer interfacial contact resistance determination

Sigrid Lædre [a], Corneliu M. Craciunescu [b], Thulile Khoza [a], Nicolae Vaszilcsin [b], Andrea Kellenberger [b,*], Vlad Bolocan [b], Ion Mitelea [b], Aurel Ercuta [b]

[a] SINTEF Industry, 7465, Trondheim, Norway
[b] Politehnica University of Timisoara, RO-300006, Timisoara, Romania

HIGHLIGHTS

- Reliability of ICR measurements depends on the position of the current contacts.
- Central and mid-edge positions for voltage drop reading are also compared.
- Method with four currents path and central position for reading the voltage drop.
- The method assures more uniform current flow and potential distribution.

ARTICLE INFO

Keywords:
Proton exchange membrane fuel cell
Bipolar plate
Gas diffusion layer
Interfacial contact resistance
Carbon paper
Stainless steel

ABSTRACT

The interfacial contact resistance ($ICR_{BPP\text{-}GDL}$) between the bipolar plates (BPPs) and gas diffusion layers (GDLs) plays a major role in proton exchange membrane-fuel cells (PEMFCs) efficiency. Accordingly, materials selection based on *ex-situ* $ICR_{BPP\text{-}GDL}$ determination is a useful tool, provided accurate through-plane resistance measurements are ensured; in this sense, an experimental study was conducted. To this end, two square-shaped samples of equal areas, one from stainless steel (a low cost BPP material), and one from carbon paper (a widely used GDL material) were placed (both separately, and stacked) between two planar Cu electrodes, and the through-plane resistance of the as-formed measuring cell was determined at various applied clamping pressures (p). It was found that although falling into the same order of magnitude (tens of mΩ cm^2), the results extracted from these measurements as $ICR_{BPP\text{-}GDL}$ (p) are affected by the non-uniformity of the current flow through the measuring cell, and also by the position of the voltage pick-up contacts. It was concluded that if reasonably uniform path is ensured for the biasing current by splitting this into four equal currents, and if central points are used for voltage pick-up, realistic results are expected.

1. Introduction

Hydrogen is foreseen to play an important role in the future sustainable society if the goals for reduction of emissions set out by the IPCC climate report (https://www.un.org/en/climatechange/reports) as well as the COP 26 agreement (https://ukcop26.org) are to be reached. Proton Exchange Membrane Fuel Cells (PEMFCs) produce electricity by converting hydrogen and oxygen into water, rendering it a zero emission technology. The Bipolar Plates (BPP) are essential components when combining single fuel cells into a stack. In addition to being a physical separator between single cells, the bipolar plates have several important tasks: they manage the gas and water within the stack, remove heat from active areas and conduct current in between single cells in the stack. In order to be cost competitive while also comply with all these demands in the acidic PEMFC environment, the bipolar plates need to have high corrosion resistance and mechanical strength. In addition, a key target listed in Table 3.4.8 from the 2016 edition of the US Department of Energy Multiyear R D& D Plan (https://www.osti.gov/biblio/1219578-multiyear-research-development-demonstration-plan), is that the interfacial contact resistance ($ICR_{BPP\text{-}GDL}$) between the BPP and the Gas Diffusion Layer (GDL) should be less than 10 mΩ cm^2 for internal power loss minimization reasons. In this sense, *ex-situ* $ICR_{BPP\text{-}GDL}$ determination

* Corresponding author.
E-mail address: andrea.kellenberger@upt.ro (A. Kellenberger).

https://doi.org/10.1016/j.jpowsour.2022.231275
Received 26 November 2021; Received in revised form 3 March 2022; Accepted 5 March 2022
Available online 17 March 2022

has become a common preliminary test [1–19] used to identify potential BPP candidates. Whereas stainless steel is nowadays a material of primary interest for low cost BPPs [20], carbon paper is often used for GDLs [21].

Several studies focused on *ex-situ* $ICR_{BPP\text{-}GDL}$ determination have revealed the fact that measurements conducted on similar materials under similar clamping pressure conditions do not always render similar results (see Table. 3 in Ref. [20] for a comprehensive review): thus, for non-coated stainless steel BPPs and carbon paper GDLs assemblies subjected to compacting forces like those applied in the operating fuel cell stacks (140 N cm^{-2} to 150 N cm^{-2}), interfacial contact resistances from tens to hundreds of mΩ cm^2 were reported. Such a spread in the $ICR_{BPP\text{-}GDL}$ values is primarily attributed to some inherent differences in the surface morphology or in the chemical composition of the BPP and/or GDL samples used in these tests, but it still remains of interest to find out if and to what extent, a certain widely accepted assumption (in fact, a hidden hypothesis) may deviate the measurement procedure from a realistic approach. According to this assumption, the biasing electric current is regarded as flowing uniformly through the measuring cell (built from thin planar samples stacked between two planar electrodes), which means that the macroscopic Ohms' law U = R·I holds regardless the cell geometry (here, U is the voltage drop across the cell, I is the current through this, and R is the cell resistance). In fact, if the results from measurements based on this assumption may be accepted as reliable for specimens of large length-to-transverse size ratio and uniform cross section, these results become questionable when this ratio is inverted (i.e. when flat measuring cells are used). In addition, it is often assumed that if samples from similar BPP and GDL materials are used, similar $ICR_{BPP\text{-}GDL}$ results are expected, regardless their shape (rectangular, circular, etc.). One may then conclude that the reliability of low resistance measurements on conducting plates will not be affected by the positions of the biasing current contacts and/or of the voltage pick-up points. Finally, it is often assumed that the through-plane resistances of the BPP and GDL samples are negligibly small compared to $R_{BPP\text{-}GDL}$ (to some extent this is justified for metal BPP samples).

For measuring procedures and devices, various solutions (more or less adapted for high precision through-plane resistance measurements), from DC (Kelvin-type micro-ohmmeter [15,22,23] or Ammeter-Voltmeter (A-V) circuit [1,24]), to impedance [25] or lock-in [6] a.c. techniques were used.

The present work aims to bring *ex-situ* experimental evidence of the fact that using biasing currents of different degrees of uniformity, and different positions of the voltage pick-up contacts will lead to different results in interfacial contact resistance measurements. Square-shaped copper electrodes, stainless steel bipolar plates and carbon paper gas diffusion layers were used. In order to ensure sufficiently high precision results an original equipment was built, and a numerical signal processing procedure was designed; the final results are presented as the clamping pressure dependence of the $ICR_{BPP\text{-}GDL}$.

2. Experimental work

2.1. The principle of the method

Consider a pair of identical planar electrodes (E_1, E_2), a BPP sample, and a GDL sample, from which a measuring cell is built in three different serial configurations (Fig. 1). The cell is subjected to a clamping pressure (p), and its transverse electrical resistance (presumably pressure dependent) is measured in each of the three stacking variants; let $R_1(p)$, $R_2(p)$, and $R_3(p)$ the corresponding quantities. Then, denoting by $2R_E(p)$, $R_{BPP}(p)$, and $R_{GDL}(p)$ the through-plane (bulk) resistances of the E_1, E_2 pair, BPP, and GDL, respectively, and by $R_{E\text{-}BPP}(p)$, $R_{E\text{-}GDL}(p)$, and $R_{BPP\text{-}GDL}(p)$ the interfacial contact resistances between these cell components, if uniform flow of the biasing current is assumed, the following relations:

$$\begin{aligned}
&(a)\quad 2R_E(p) + R_{BPP}(p) + 2R_{E-BPP}(p) = R_1(p)\\
&(b)\quad 2R_E(p) + R_{GDL}(p) + 2R_{E-GDL}(p) = R_2(p)\\
&(c)\quad 2R_E(p) + R_{BPP}(p) + R_{GDL}(p) + R_{E-BPP}(p) + R_{E-GDL}(p) + \quad R_{BPP-GDL}(p) = R_3(p)
\end{aligned} \tag{1}$$

result. Furthermore, by eliminating $R_E(p)$, and substituting $R_{E\text{-}BPP}(p)$, and $R_{E\text{-}GDL}(p)$ one obtains:

$$R_{BPP-GDL}(p) = R_3(p) - \frac{1}{2}[R_1(p) + R_2(p) + R_{BPP}(p) + R_{GDL}(p)] \tag{2}$$

Here, $R_{BPP}(p)$ and $R_{GDL}(p)$, will be treated separately, with reference to the BPP, and GDL samples used in our measurements, a stainless steel plate, and a carbon paper, respectively. As it will be shown in Section 3 (Results and discussion), the as-measured cell resistance (R_{cell}) values i.e. $R_1(p)$, $R_2(p)$, and $R_3(p)$ lie in the range of tens of mΩ, which is the usual case. In what concerns the BPP, a calculation based on manufacturer-supplied data yields through-plane resistance values in the μΩ range, which is by four orders of magnitude less than R_{cell}, thus making reasonable the assumption of negligibly small contribution to Eq. (2). In what concerns the GDL sample, a similar calculation yields for the through-plane resistance values only by one order of magnitude less than R_{cell}, which means that $R_{GDL}(p)$ cannot be neglected in Eq. (2). Yet a simplification may still be made, based on the observed fact that clamping pressure values in the MPa range (like in real PEMFC stacks) will cause permanent thickness reduction (by plastic deformation) of the carbon paper, which in turn will decrease the material compressibility, thus reducing the effect of subsequent clamping pressure. Hence, if the fact that the major contribution of the GDL sample to R_{cell} is of interfacial contact nature is taken into account, replacing the $R_{GDL}(p)$ dependence with a constant value, say R_{GDL}, is justified. Under these circumstances, Eq. (2) may be rewritten as:

$$R_{BPP-GDL}(p) = R_3(p) - \frac{1}{2}[R_1(p) + R_2(p) - R_{GDL}] \tag{3}$$

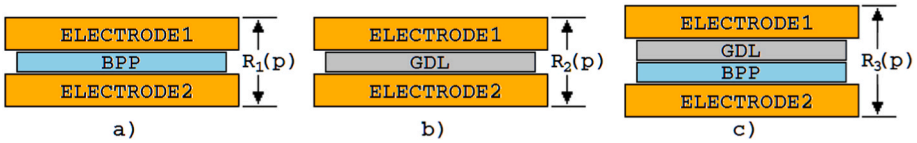

Fig. 1. The three measuring cell configurations considered in our experiments; all the resistances contributing to the cell through-plane resistances R1(p), R2(p), and R3(p) are connected in series.

The above measuring scenario (which will be applied in the experiment) involves approximations suitable for thin BPP and GDL samples. However, for plates of larger thickness $R_{BPP}(p)$, and $R_{GDL}(p)$ determination may be considered. In this case, under uniform distribution of the current density through the plates, R_{BPP} and R_{GDL} may be determined in a way similar to that first proposed by Sadeghifar [22]. This consists in repeating the two single-plate measurements (see Fig. 1 a, and Fig. 1b), with BPP, and GDL samples of the same geometry, grade, and surface condition, but having the thickness modified say, by factors α and β, respectively, which means that the new through-plane resistances will be $\alpha\, R_{BPP}$, and $\beta\, R_{GDL}$. Then, if $R_4(p)$ and $R_5(p)$ are the new as-measured cell resistances, the first two Eq. (1) will be replaced with:

$$\begin{array}{ll}(a') & 2R_E(p)+\alpha R_{BPP}(p)+2R_{E-BPP}(p)=R_4(p)\\ (b') & 2R_E(p)+\beta R_{GDL}(p)+2R_{E-GDL}(p)=R_5(p)\end{array} \tag{4}$$

and Eq. (2) becomes:

$$R_{BPP-GDL}(p)=R_3\left(p\right)-\frac{R_1(p)+R_2(p)}{2}-\frac{R_1(p)-R_4(p)}{2(1-\alpha)}-\frac{R_2(p)-R_5(p)}{2(1-\beta)} \tag{5}$$

Finally, if the BPP and GDL samples have the same surface area, say S_p, the interfacial contact resistance will be calculated as:

$$ICR_{BPP-GDL}(p)=S_p\cdot R_{BPP-GDL}(p) \tag{6}$$

Clearly, the small values (mΩs to tens of mΩs) of the through-plane resistance of such cells will require accurate measurements; to this end, an experimental setup, presented in the next section, was designed.

2.2. Through-plane measurements setup

In Fig. 2 the paths of the biasing current flow through the measuring cell, and the contacts for the voltage reading are indicated. Thus, two *single current* paths (Fig. 2a, and b), and a *four currents* path (Fig. 2c) were considered for biasing, and two pairs of contact points placed in the *central* (C,C′) and *mid-edge* (M,M′) positions were used for reading the voltage drops across the cell, $u_{CC'}$, and $u_{MM'}$, respectively.

As the more precisely the cell resistance is measured, the more accurate ICR values will result, an original solution for small resistance a.c. measurements was proposed to this end; in Fig. 3 the experimental setup diagram is shown. Here, the AF oscillator KH5700 (KROHN-HITTE) is used to generate a low frequency a.c. voltage signal (30.17 Hz, triangular waveform), which is amplified by means of the bipolar amplifier BOP50-2 M (KEPCO) having a serial circuit as a load. The load circuit includes a current limiting resistor ($R_L = 68.00\ \Omega$), the measuring cell connected through a configurable network of eight identical resistors ($R_e = 2.00\ \Omega$, exceeding by two orders of magnitude the cell resistance), and a calibrated current sensing resistor ($R_i = 1.003\ \Omega$). By means of keys k_1, k_2, …$k_{3'}$, $k_{4'}$ all the biasing combinations depicted in Fig. 2 may be rendered, whereas in all the biasing variants the voltage drop $u_i(t) = R_i \bullet i(t)$ will be considered as a direct measure of the current $i(t)$ flowing through the cell.

A pair of 50 mm × 50 mm x 5 mm Cu electrodes, a 30 mm × 30 mm x 2.00 mm AISI 446 stainless steel (www.metalcor.de/en/datenblatt/54/) BPP sample, and a 30 mm × 30 mm x 350 μm Spectracarb™ 2050A-1550 carbon paper (http://www.eftspectracorp.com/forms%202016/TDS00202282050A155029.pdf) GDL were used in building the measuring cell. The GDL sample was subjected to several loading cycles up to 3.8 MPa, which caused thickness reduction to 260 μm. The contact faces of the Cu electrodes, and the top and bottom faces of the BPP sample were polished using KLINGSPOR™ PS11A-P600 SiC grinding paper (https://www.klingspor.co.uk/products/abrasive-sheets/ps-11-a/pdf); clearly, higher grit ensures finer surface roughness, and therefore lower ICR (e.g. Ref. [26]), but our choice was to maintain surface condition close to that in industrial PEMFCs. The cell components were then cleaned in ultrasound acetone bath prior to mounting.

During measurements, the cell was subjected to clamping pressures from 0.57 MPa to 1.90 MPa applied in 0.19 MPa steps by means of a P. I.88.00 (OMEC) hydraulic press. Voltages $u_i(t)$, $u_{CC'}(t)$, and $u_{MM'}(t)$ are collected and then processed in the DIFF.AMP.UNIT containing 3 d.c.-coupled differential amplifiers of gains $g_i = 10$, $g_c = 100$, and $g_m = 100$, respectively. The unit was built from precision electronic parts, including a 10 MHz bandwidth operational amplifier LF357 (NATIONAL) per channel, and 0.5% precision resistors. The output signals $g_i \bullet u_i(t)$, $g_c \bullet u_{CC'}(t)$, and $g_m \bullet u_{MM'}(t)$ were then recorded as ASCII files via PC-controlled 16 bit resolution analog-to-digital conversion, by means of the ECON series DT 9816 (DATA TRANSLATION) simultaneous channels data acquisition board.

3. Results and discussion

The as recorded output signals were digitally processed, in order to obtain the families $u_{CC'}(i)_{p\,=\,const}$, and $u_{MM'}(i)_{p\,=\,const}$ of characteristics. The results as plotted in Fig. 4, Fig. 5, and Fig. 6 indicate the fact that unlike in the ideal case, in which these characteristics are expected to coincide (one by one, and for the same given sample and clamping pressure), differences in slope occur both for the three biasing current paths and for the two positions of the voltage pick-up contacts. As expected, the slopes decrease as the clamping pressure increases in all the biasing cases (the arrows in these figures visually indicate the pressure increase), thus confirming the progressive strengthen of the contact between the measuring cell components. Yet, it is worth noting that these differences in slope are notably smaller in the case of the *four currents* biasing path variant, in other words in the case of a better uniformity of the biasing current flow. It is also confirmed that the major contribution to the through-plane resistance of the measuring cell is provided by the interfacial contact between the constitutive parts (E_1, E_2, BPP, and GDL).

As visible from Figs. 4, Fig.5, and Fig.6, the $u_{MM'}(i)$ and $u_{CC'}(i)$ characteristics are linear. Accordingly, accurate determination of the cell through-plane resistance values was performed by least squares minimization fitting these characteristics to robust straight line, using the form:

$$y = a + b\cdot x \tag{7}$$

where y is the voltage drop across the cell, x is the current through this, the intercept a of the ordinate axis is the output voltage error component

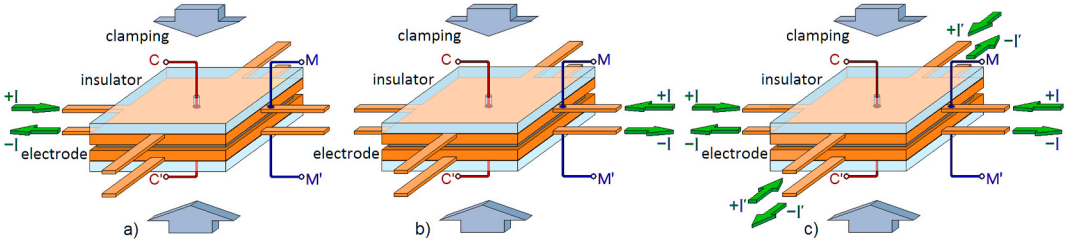

Fig. 2. The paths of the biasing current (i), and the voltage pick-up contacts considered in our study: a) *single current* with $u_{MM'}$ reading similar to the classical A-V method, b) *single current* with $u_{MM'}$ reading similar to the 4 wires (Kelvin) Ohmmeter method, and c) *four currents* (i' = i/4).

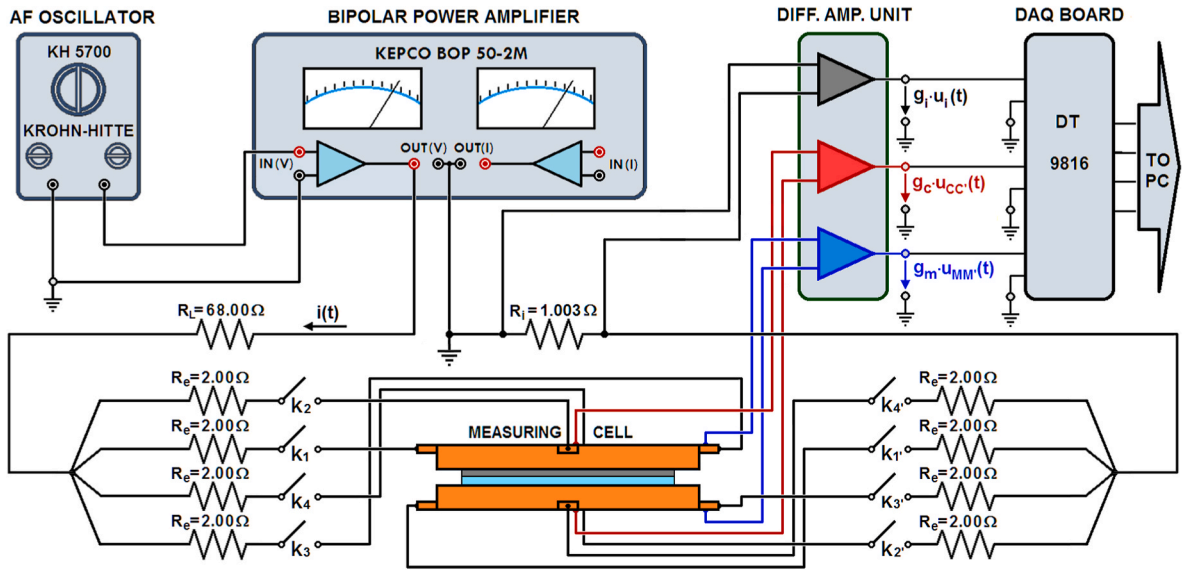

Fig. 3. Experimental setup for accurate ICR measurements (schematic); by means of keys k_1, k_2, …$k_{3'}$, $k_{4'}$ the biasing currents paths are controlled: k_1, $k_{1'}$ closed renders the connections in Fig. 2.a), k_3, $k_{3'}$ closed those in Fig. 2.b), and all the keys closed yields the case in Fig. 2.c).

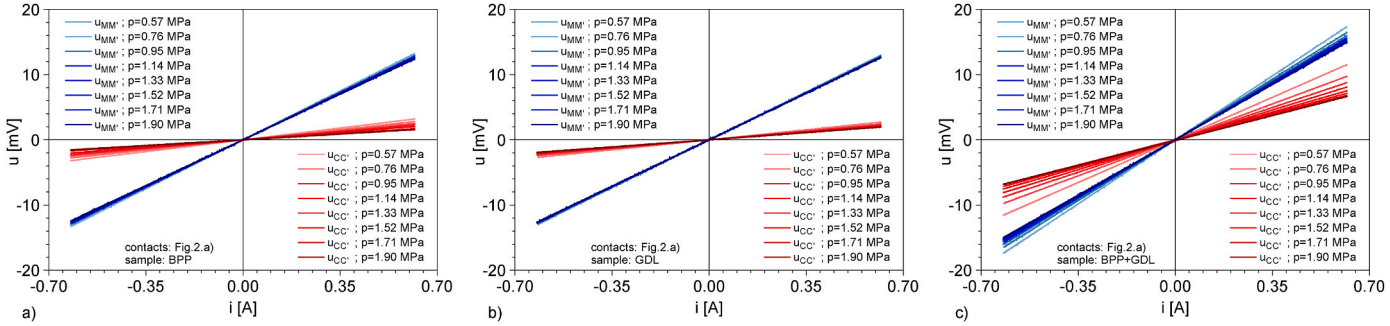

Fig. 4. The $u_{MM'}(i)_{p\,=\,const}$, and $u_{CC'}(i)_{p\,=\,const}$ families of characteristics for the *single current* biasing path depicted in Fig. 2.a), using: a) the BPP sample, b) the GDL sample, and c) the BPP + GDL stack as a sample.

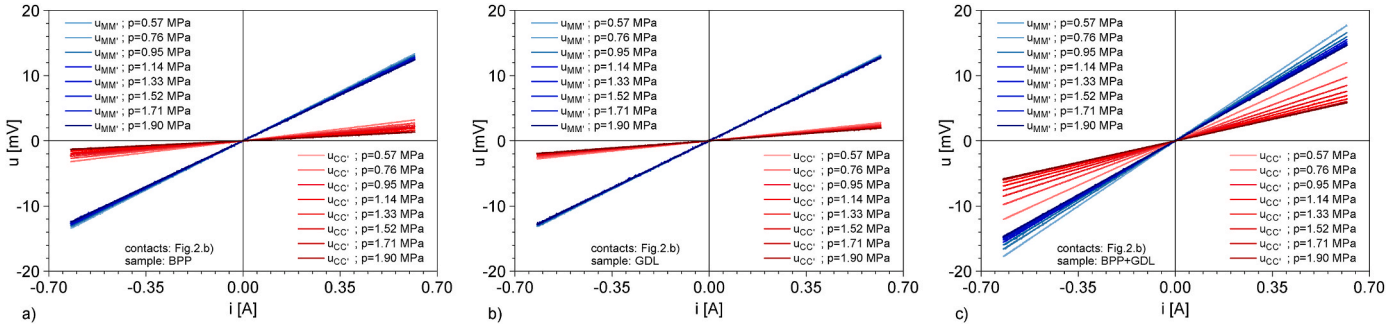

Fig. 5. The $u_{MM'}(i)_{p\,=\,const}$, and $u_{CC'}(i)_{p\,=\,const}$ families of characteristics for the *single current* biasing path depicted in Fig. 2.b), using: a) the BPP sample, b) the GDL sample, and c) the BPP + GDL stack as a sample.

(here, in the mV range) caused by imperfect input offset voltage cancellation, and the slope *b* is the cell resistance; a coefficient of determination (r^2) exceeding 0.9998 resulted in all cases ($r^2 = 1$ corresponds to perfect match of the fitting function to the experimental data), which confirms the goodness of the fit, as well as the accuracy of the measuring method.

Once the cell resistance values were determined for all the six measuring variants, the $R_1(p)$, $R_2(p)$, and $R_3(p)$ dependences were obtained; in Fig. 7 the results are plotted. One can remark that although the cell resistance values fall into the usually reported numerical range (tens of mΩ), significant differences occur between the R_{cell} values calculated using the $u_{MM'}$ data from any of the two *single current* biasing paths, compared to those from the *four currents* path (Fig. 7a,b,c); on the contrary, the R_{cell} values calculated using the $u_{CC'}$ data are considerably closer, regardless the biasing path (Fig. 7d,e,f).

These differences are consistent with the fact that the electrodes are larger in size than the sample plates (a common practice [2,5,13,16,27,28]), which complicates the current flow through the electrodes. Thus,

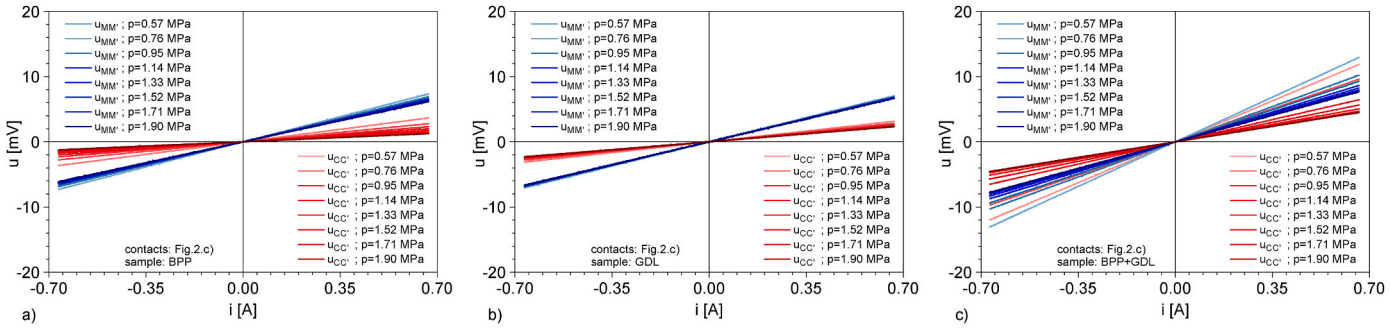

Fig. 6. The $u_{MM'}(i)_{p\,=\,const}$ and $u_{CC'}(i)_{p\,=\,const}$ families of characteristics for the *four currents* biasing path depicted in Fig. 2.c), using: a) the BPP sample, b) the GDL sample, and c) the BPP + GDL stack as a sample.

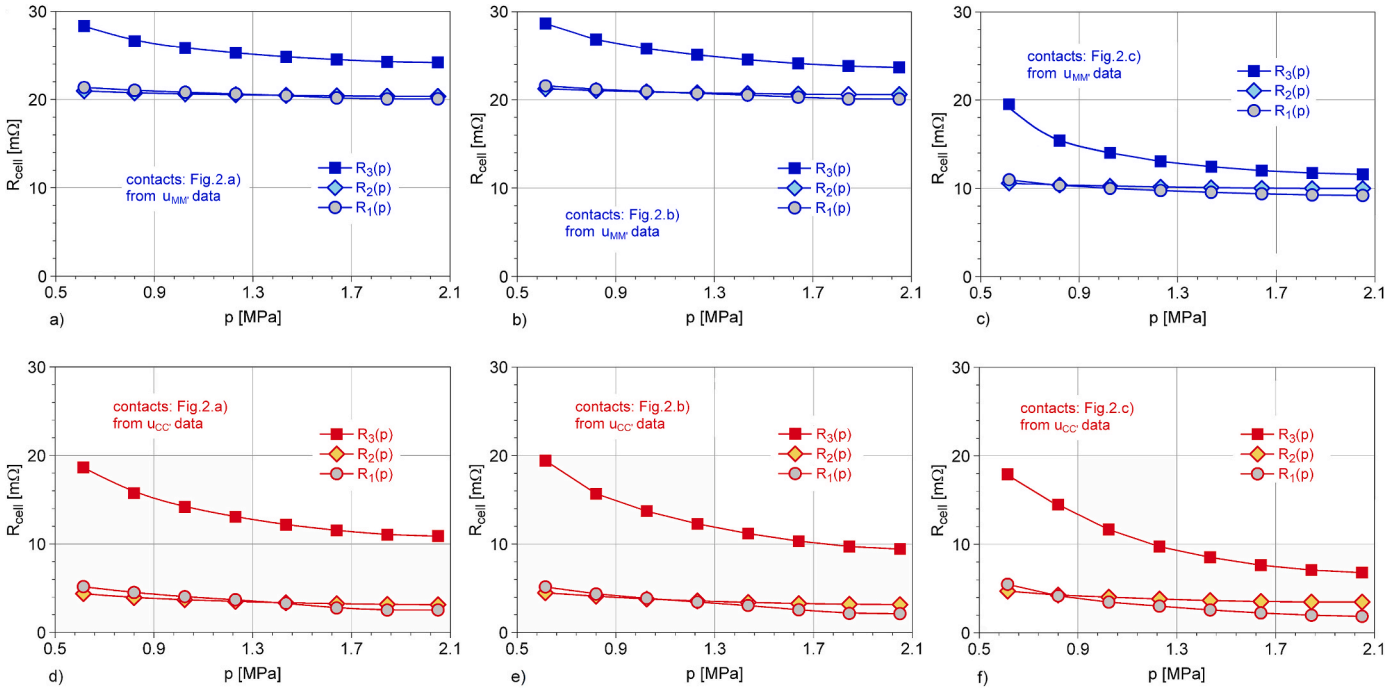

Fig. 7. Pressure dependence of the measuring cell resistance as derived from the $u_{MM'}(i)_{p\,=\,const}$ and $u_{CC'}(i)_{p\,=\,const}$ families of characteristics; the *single current* and *four currents* biasing paths in Fig. 2 were used.

an *effective in-plane resistance* connected in series with the through-plane cell resistance between the $u_{CC'}$ pick-up contacts, and attributed to the current flow from the biasing contacts (at the electrode edge) towards the central area (overlapping the samples) may be assumed. Accordingly, the voltage drop across this serial resistance may explain the differences between the $u_{MM'}$ and $u_{CC'}$ data sets (see Figs. 4–6), as well as the differences between the calculated $R_{cell}(p)$ dependences plotted in Fig. 7a,b,c, and those plotted in Fig. 7d,e,f. An explanation to the fact that these differences are smaller in the case of the *four currents* path is that the biasing current flow is eased when injected throug four symmetrically placed contacts. In what concerns the R_{cell} decrease with increasing compression, this is mainly attributed to the enhancement of the interfacial contact between the components of the measuring cell, and the fact that $R_2(p)$ the resistance of the cell containing the GDL

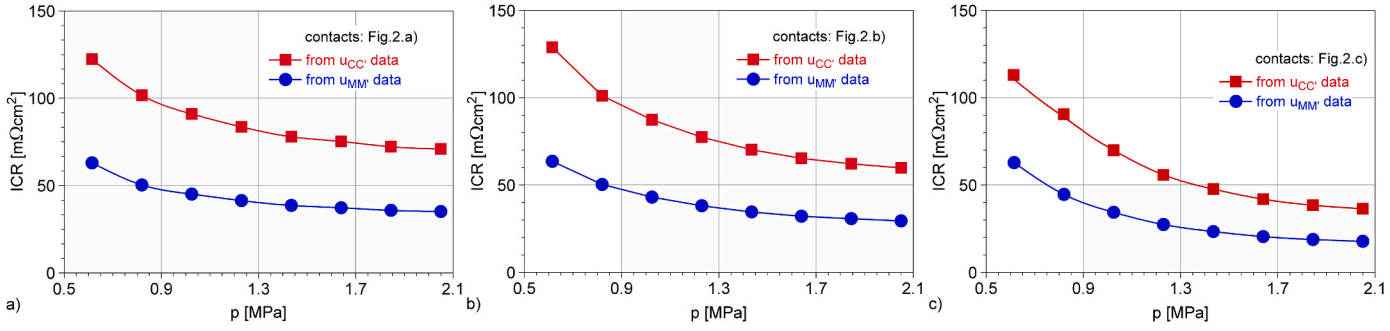

Fig. 8. $ICR_{BPP\text{-}GDL}(p)$ dependence calculated from the experimental data plotted in Fig. 7.

sample (diamond symbols in Fig. 7) exhibits the lowest decay compared to $R_1(p)$, and $R_3(p)$ is ascribed to the fact that the above contact enhancement takes place at pressures below the experimental range.

Finally, using Eqs. (3) and (6), the $ICR_{BPP\text{-}GDL}(p)$ dependences were calculated from the $R_1(p)$, $R_2(p)$, and $R_3(p)$ data, and plotted in Fig. 8. Calculations were performed using 1.09 mΩ for R_{GDL}, as derived from Eqs. (9) and (10) in Ref. [8], and starting from the 1.7 mΩ value derived from manufacturer's data (Spectracarb™ 2050A-1550 carbon paper exhibits 350 μm thickness, 78% porosity, and 15 mΩ cm^2 specific through-plane resistance at 200 kPa compression), as an effect of the thickness reduction (by plastic deformation) from 350 μm to 260 μm, caused by preliminary loading. However, due to actually small contribution to R_{cell}, any further pressure dependence of this resistance was neglected.

As a first observation, unlike the $R_{cell}(p)$ dependences, the $ICR_{BPP\text{-}GDL}(p)$ dependences calculated from the $u_{CC'}$ data are greater than those from the $u_{MM'}$ data (note that these two signals were always recorded simultaneously), regardless the current biasing variant. To the present, there is no evidence that this is a general rule, or it depends on the surface condition of the cell components; the question remains open.

As a second observation, the *four currents path* always leads to lower $ICR_{BPP\text{-}GDL}$ values compared to their single current path correspondents.

Under these circumstances, the *four currents* biasing path in conjunction with the $u_{CC'}(t)$ voltage pick-up option appears to be the most realistic ICR measurement option.

4. Conclusions

Ex-situ determination of the clamping pressure-dependent ICR between stainless steel BPP and carbon paper GDL was performed in square plates geometry, and four measuring combinations: two different paths (*single current* and *four currents*) of the biasing electrical current, and two different combinations (*mid-edge* or *central*) of the voltage pick-up contacts positions. To this end, an original setup, suitable for precision measurements of small through-plane electrical resistance, and enabling simultaneous records of the biasing current (triangular waveform, 31.7 Hz frequency, 0.68 A amplitude) and of the two voltage pick-up signals, was designed. The measurements have shown that, depending on the current biasing and voltage measuring contact points combination, notable differences (exceeding 100% in several cases) may occur between the as-determined ICR values, yet all within the conventional order of magnitude (e.g. tens of mΩ cm^2 for stainless steel BPP/carbon paper GDL pair of samples). Such differences are primarily attributed to the different degrees of non-uniformity (produced by the positions of the biasing contact points) of the current flow through the measuring cell. It is expected that more realistic results may be obtained if the uniformity of the current flow will be improved by extending the number of the biasing points, by increasing the thickness of the Cu electrodes, and also by building measuring cells of cylindrical symmetry; a research aiming to bring new insights is in progress.

CRediT authorship contribution statement

Sigrid Lædre: Conceptualization, Writing – review & editing, Resources. **Corneliu M. Craciunescu:** Conceptualization, Methodology, Supervision. **Thulile Khoza:** Writing – review & editing, Resources. **Nicolae Vaszilcsin:** Methodology, Resources. **Andrea Kellenberger:** Writing – review & editing, Methodology, Resources. **Vlad Bolocan:** Investigation, Resources. **Ion Mitelea:** Resources. **Aurel Ercuta:** Investigation, Writing – original draft.

Declaration of competing interest

The authors declare that they have no known competing financial interests or personal relationships that could have appeared to influence the work reported in this paper.

Acknowledgment

The research leading to these results has received funding from the EEA Grants 2014–2021, under Project contract no. 2/2019 CoDe-PEM (EEA RO–NO–2018-0502).

References

[1] H. Wang, M.A. Sweikart, J.A. Turner, Stainless steel as bipolar plate material for polymer electrolyte membrane fuel cells, J. Power Sources 115 (2) (2003) 243–251, https://doi.org/10.1016/S0378-7753(03)00023-5.
[2] V. Mishra, F. Yang, R. Pitchumani, Measurement and prediction of electrical contact resistance between gas diffusion layers and bipolar plate for applications to PEM fuel cells, J. Fuel Cell Sci. Technol. 1 (2004) 2–9, https://doi.org/10.1115/1.1782917.
[3] N. Cunningham, M. Lefevre, G. Lebrun, J.-P. Dodelet, Measuring the through-plane electrical resistivity of bipolar plates (apparatus and methods), J. Power Sources 143 (2005) 93–102, https://doi.org/10.1016/j.jpowsour.2004.11.062.
[4] W.R. Chang, J.J. Hwang, F.B. Weng, S.H. Chan, Effect of clamping pressure on the performance of a PEM fuel cell, J. Power Sources 166 (1) (2007) 149–154, https://doi.org/10.1016/j.jpowsour.2007.01.015.
[5] T. Fukutsuka, T. Yamaguchi, S.-I. Miyano, Y. Matsuo, Y. Sugie, Z. Ogumi, Carbon-coated stainless steel as PEFC bipolar plate material, J. Power Sources 174 (1) (2007) 199–205, https://doi.org/10.1016/j.jpowsour.2007.08.096.
[6] J. André, L. Antoni, J.-P. Petit, E. De Vito, A. Montani, Electrical contact resistance between stainless steel bipolar plate and carbon felt in PEFC: a comprehensive study, Int. J. Hydrogen Energy 34 (7) (2009) 3125–3133, https://doi.org/10.1016/j.ijhydene.2009.01.089.
[7] B. Avasarala, P. Haldar, Effect of surface roughness of composite bipolar plates on the contact resistance of a proton exchange membrane fuel cell, J. Power Sources 188 (1) (2009) 225–229, https://doi.org/10.1016/j.jpowsour.2008.11.063.
[8] O. Aydin, M. Zedda, N. Zamel, Challenges associated with measuring the intrinsic electrical conductivity, Fuel Cell. 15 (3) (2015) 537–544.
[9] P. Jendras, K. Lötsch, T. von Unwerth, Requirements and testing methods for surfaces of metallic bipolar plates for low-temperature PEM fuel cells, IOP Conf. Ser. Mater. Sci. Eng. 181 (2017), 012018, https://doi.org/10.1088/1757-899X/181/1/012018.
[10] E.F. Mine, Y. Ito, Y. Teranishi, M. Sato, T. Shimizu, Surface coating and texturing on stainless-steel plates to decrease the contact resistance by using screen printing, Int. J. Hydrogen Energy 42 (31) (2017) 20224–20229, https://doi.org/10.1016/j.ijhydene.2017.06.154.
[11] P. Liang, D. Qiu, L. Peng, P. Yi, X. Lai, Jun Ni, Contact resistance prediction of proton exchange membrane fuel cell considering fabrication characteristics of metallic bipolar plates, Energy Convers. Manag. 169 (2018) 334–344, https://doi.org/10.1016/j.enconman.2018.05.069.
[12] M. Kim, J.W. Lim, D.G. Lee, Electrical contact resistance between anode and cathode bipolar plates with respect to surface conditions, Compos. Struct. 189 (2018) 79–86, https://doi.org/10.1016/j.compstruct.2018.01.067.
[13] D. Qiu, H. Janßen, L. Peng, P. Irmscher, X. Lai, W. Lehnert, Electrical resistance and microstructure of typical gas diffusion layers for proton exchange membrane fuel cell under compression, Appl. Energy 231 (2018) 127–137, https://doi.org/10.1016/j.apenergy.2018.09.117.
[14] S. Lædre, O.E. Kongstein, A. Oedegaard, F. Seland, H. Karoliussen, Measuring in situ interfacial contact resistance in a proton exchange membrane fuel cell, J. Electrochem. Soc. 166 (13) (2019) F853–F859, https://doi.org/10.1149/2.1511912jes.
[15] H. Agarwal, R. Pandey, S.D. Bhat, Improved polymer electrolyte fuel cell performance with membrane electrode assemblies using modified metallic plate: comparative study on impact of various coatings, Int. J. Hydrogen Energy 45 (37) (2020) 18731–18742, https://doi.org/10.1016/j.ijhydene.2019.05.243.
[16] A.V. Ingle, V.S. Raja, J. Rangarajan, P. Mishra, Corrosion resistant quaternary Al-Cr-Mo-N coating on type 316L stainless steel bipolar plates for proton exchange membrane fuel cells, Int. J. Hydrogen Energy 45 (4) (2020) 3094–3107, https://doi.org/10.1016/j.ijhydene.2019.11.119.
[17] S. Proch, M. Stenström, L. Eriksson, J. Andersson, G. Sjöblom, A. Jansson, J. Westlinder, Coated stainless steel as bipolar plate material for anion exchange membrane fuel cells (AEMFCs), Int. J. Hydrogen Energy 45 (2) (2020) 1313–1324, https://doi.org/10.1016/j.ijhydene.2019.04.122.
[18] D.P. Davies, P.L. Adcock, M. Turpin, S.J. Rowen, Bipolar plate materials for solid polymer fuel cells, J. Appl. Electrochem. 30 (2000) 101–105, https://doi.org/10.1023/A:1003831406406.
[19] S. Lædre, O.E. Kongstein, A. Oedegaard, F. Seland, H. Karoliussen, The effect of pH and halides on the corrosion process of stainless steel bipolar plates for proton exchange membrane fuel cells, Int. J. Hydrogen Energy 37 (23) (2012) 18537–18546, https://doi.org/10.1016/j.ijhydene.2012.09.021.
[20] L. Yu, P. Ming, D. Yang, C. Zhang, Stainless steel bipolar plates for proton exchange membrane fuel cells: Materials, flow channel design and forming processes, J. Power Sources 451 (2020), 227783, https://doi.org/10.1016/j.jpowsour.2020.227783.
[21] A. El-kharouf, T.J. Mason, D.J.L. Brett, B. Pollet G., Ex-situ characterisation of gas diffusion layers for proton exchange membrane fuel cells, J. Power Sources 218 (2012) 393–404, https://doi.org/10.1016/j.jpowsour.2012.06.099.
[22] H. Sadeghifar, In-plane and through-plane electrical conductivities and contact resistances of a Mercedes-Benz catalyst-coated membrane, gas diffusion and

microporous layers and a Ballard graphite bipolar plate: Impact of humidity, compressive load and polytetrafluoroethylene, Energy Convers. Manag. 154 (2017) 191–202, https://doi.org/10.1016/j.enconman.2017.10.060.

[23] M.S. Ismail, D.B. Ingham, L. Ma, M. Pourkashanian, The contact resistance between gas diffusion layers and bipolar plates as they are assembled in proton exchange membrane fuel cells, Renew. Energy 52 (2013) 40–45, https://doi.org/10.1016/j.renene.2012.10.025.

[24] A. Orsi, O.E. Kongstein, P.J. Hamilton, A. Oedegaard, I.H. Svenum, K. Cooke, An investigation of the typical corrosion parameters used to test polymer electrolyte fuel cell bipolar plate coatings, with titanium nitride coated stainless steel as a case study, J. Power Sources 285 (2015) 530–537, https://doi.org/10.1016/j.jpowsour.2015.03.111.

[25] H. Choi, D.J. Seo, W.Y. Choi, M.H. Lee, Y.J. Park, T.Y. Kim, Y.G. Yoon, S.-C. Yi, C.-Y. Jung, An ultralight-weight polymer electrolyte fuel cell, J. Power Sources 484 (2021), 229291, https://doi.org/10.1016/j.jpowsour.2020.229291.

[26] G. Yang, S. Yu, J. Mo, Z. Kang, Y. Dohrmann, F.A. List III, J.B. Green Jr., S.S. Babu, F.-Y. Zhang, Bipolar plate development with additive manufacturing and protective coating for durable and high-efficiency hydrogen production, J. Power Sources 396 (2018) 590–598, https://doi.org/10.1016/j.jpowsour.2018.06.078.

[27] A. Kumar, M. Ricketts, S. Hirano, Ex-situ evaluation of nanometer range gold coating on stainless steel substrate for automotive polymer electrolyte membrane fuel cell bipolar plate, J. Power Sources 195 (5) (2010) 1401–1407, https://doi.org/10.1016/j.jpowsour.2009.09.022.

[28] E.M. Gabreab, G. Hinds, S. Fearn, D. Hodgson, J. Millichamp, P.R. Shearing, D.J. L. Brett, An electrochemical treatment to improve corrosion and contact resistance of stainless steel bipolar plates used in polymer electrolyte fuel cells, J. Power Sources 245 (2014) 1014–1026, https://doi.org/10.1016/j.jpowsour.2013.07.041.